Acta Mechanica Sinica (2013) 29(3):335–347
DOI 10.1007/s10409-013-0039-x

RESEARCH PAPER

Optimization of $LiMn_2O_4$ electrode properties in a gradient- and surrogate-based framework

Wenbo Du · Nansi Xue · Amit Gupta · Ann M. Sastry · Joaquim R. R. A. Martins · Wei Shyy

Received: 26 February 2013 / Accepted: 8 April 2013

Abstract In this study, the effects of discharge rate and $LiMn_2O_4$ cathode properties (thickness, porosity, particle size, and solid-state diffusivity and conductivity) on the gravimetric energy and power density of a lithium-ion battery cell are analyzed simultaneously using a cell-level model. Surrogate-based analysis tools are applied to simulation data to construct educed-order models, which are in turn used to perform global sensitivity analysis to compare the relative importance of cathode properties. Based on these results, the cell is then optimized for several distinct physical scenarios using gradient-based methods. The complementary nature of the gradient- and surrogate-based tools is demonstrated by establishing proper bounds and constraints with the surrogate model, and then obtaining accurate optimized solutions with the gradient-based optimizer. These optimal solutions enable the quantification of the tradeoffs between energy and power density, and the effect of optimizing the electrode thickness and porosity. In conjunction with known guidelines, the numerical optimization framework developed herein can be applied directly to cell and pack design.

W. Du · N. Xue · A. Gupta · J. R. R. A. Martins · W. Shyy (✉)
Department of Aerospace Engineering,
University of Michigan, Ann Arbor, Michigan 48109, USA
e-mail: weishyy@ust.hk

A. Gupta
Department of Mechanical Engineering,
Indian Institute of Technology, New Delhi, India

A. M. Sastry
Department of Mechanical Engineering,
University of Michigan, Ann Arbor, Michigan 48109, USA

W. Shyy
Department of Mechanical Engineering,
Hong Kong University of Science and Technology
Clear Water Bay, Hong Kong, China

Keywords Lithium-ion battery · Optimization · Surrogate modeling · Porous electrode model

1 Introduction

Lithium-ion batteries have attracted significant interest in recent years due to their high achievable gravimetric and volumetric energy densities, making them ideal for a wide range of applications, including portable electronics, electric vehicles, and aerospace systems such as micro-aerial vehicles [1]. A better understanding of the impact of design parameters on overall battery performance can provide guidelines and benchmarks for tailoring battery design to different applications. However, due to the disparate length and time scales over which the physical processes in a lithium-ion battery occur, as well as the complexity of the entire system, the overall performance of the battery system depends on a large number of parameters. Therefore, optimization of a lithium-ion battery is only possible in an appropriate mathematical framework. A critical step towards the optimization of a full battery pack can be taken by investigating the effects of several key parameters on a single cell by mapping the cell performance over a sufficiently broad design space to encompass a wide range of physical situations.

Through various experimental and numerical studies, cell performance has been found to depend strongly on a large number of operational, morphological, and material-dependent parameters [2–7]. Lu and Lin [2] have found experimentally that the capacity and coulomb efficiency of lithium manganese oxide particles increase substantially as the particle size is reduced. Similarly, Drezen et al. [3] found that the size of lithium manganese phosphate particles in a cathode has a critical influence on the cell performance. Tran et al. [4] investigated the effect of cycling rate on the measured capacity of graphite anode particles, concluding that the rate effect differs considerably for different-sized particles. Garcia et al. [5] used simulations to investigate the effects of particle size and diffusivity on cell performance. It

was demonstrated that performance improves with increasing diffusivity and decreasing particle size, and that the morphology of the particle aggregates also plays an important role. Darling and Newman [6] also used simulations to examine the effect of particle size distribution. A uniform size distribution was found to maximize capacity for different cycling rates. The effect of introducing conductive additives to alter the electrode material properties was also investigated by Ahn et al. [7]. It was found that metal fibers helped enhance capacity and high rate capability, while exhibiting minimal capacity loss. Differences in operating conditions and modeling parameters in these and other studies suggest a need for a numerical framework suitable for simultaneously analyzing a large number of independent parameters.

Much progress has also been made in the development of modeling tools to analyze the behavior of lithium-ion batteries, including the development of single-particle models [8, 9], equivalent circuit models [10, 11], capacity-fade models [12], microscopic models [13–15], and 3-D models [16]. Recently developed reformulated models [17, 18] have facilitated cell design by improving the computational efficiency of simulations, allowing for the optimization of porosity to maximize energy density [19]. Other recent efforts have taken a system engineering perspective to account for a wide range of physical phenomena [20]. However, despite these developments, there remains a critical need to establish effective methods for systematically examining the role of key properties such as the cathode composition and transport properties on overall cell performance. Cell design is still often based on qualitative principles in practice (for example, it has been established that thinner electrodes should be used for high power and thicker electrodes for high energy [21]), and makes limited use of formal design optimization. This is likely because, despite the possible gains in performance, optimization is often difficult to implement in the design process. For example, although various optimization algorithms have been developed, they typically require a well-defined problem with established bounds and constraints on the design variables. Additional challenges include identifying multiple regions of good or poor performance, and comparing the relative importance of multiple variables over large design ranges. Furthermore, a global perspective of the design space is often required to account for local optima in the presence of varying operational conditions such as those encountered during the life of real battery cells. Attempts to mitigate these limitations often include individual parametric studies [2–7, 22], which become problematic for problems involving multiple design variables due to inefficiency.

To address the limitations of traditional design approaches, more sophisticated numerical tools are necessary. Both gradient-based [23] and gradient-free optimization methods [24, 25] have been shown to be effective at locating optima for a wide range of well-defined problems. In particular, gradient-based optimization methods have been shown to be more efficient and capable of handling a larger number of design variables than gradient-free methods for smooth objective functions [26]. In order to fully utilize the capabilities of these algorithms, a numerical modeling framework capable of resolving the aforementioned difficulties to optimization is required. One option is the surrogate-based framework, which systematically analyzes the effects of multiple design variables simultaneously to efficiently map the design space [27]. The surrogate-based framework has been applied to a number of engineering problems [28, 29], including studying intercalation-induced stress in single $LiMn_2O_4$ particles [14], and can also be used to compare the global sensitivity to a wide range of inputs and assess the tradeoffs between multiple competing objectives, which can greatly facilitate cell optimization by identifying key regions of interest in the global design space. Given the limitations of conventional approaches for performing cell design, we define the following objectives in this work:

(1) Examine the role of multiple design variables on cell performance by varying all parameters simultaneously within the surrogate-based framework to construct reduced-order models;

(2) Quantify the relative impact of each variable within the selected design ranges to reduce the problem complexity and establish the necessary bounds required for optimization;

(3) Compare the relative merits of the two approaches for optimizing several distinct design scenarios, and

(4) Quantify the tradeoffs between competing objectives (energy and power) by constructing Pareto fronts.

Ultimately, in this study we seek to demonstrate the utility of efficient numerical methods for enhancing cell and battery design. In particular, the relative sensitivities and tradeoffs between multiple objectives are difficult to quantify without the appropriate computational tools. Here, the design variables of interest concern the operation (cycling rate), material properties (diffusion coefficient and electronic conductivity of active solid in the cathode), and configuration (particle size, porosity, and thickness of the cathode) of a lithium-ion cell. The objective functions considered in the optimization are the mass-specific energy and power (also known as the gravimetric energy and power density, respectively). While the dependence of specific energy on cycling rate, particle size, diffusivity, and conductivity has been examined previously [29], the mapping of the design space was not used to perform any cell design optimization, since the specific energy showed a monotonic trend with respect to each of the parameters considered. In contrast, the inclusion of electrode thickness and porosity contribute additional interactions between design variables and competing effects on the objective function. For example, the specific energy may be expected to increase with a greater composition of active solid in the porous electrode material, which increases the capacity. However, this increase in active solid comes at the

cost of reducing the amount of liquid electrolyte, which then decreases the overall ion transport capability of the cell. Similarly, a thick electrode may be favored to increase the capacity of the cell, but at high cycling rates the diffusivity of the material may be insufficient to utilize the additional material, resulting in insufficient gains in total energy to compensate for the additional mass. The design ranges of the cycling rate and diffusion coefficient have been expanded in this study to better correspond to electric vehicle requirements.

2 Methodology

2.1 Battery cell model

In this study, the galvanostatic discharge of a cell consisting of a $LiMn_2O_4$ cathode and graphite anode is modeled using a pseudo-2D model based on porous electrode and concentrated solution theory. This model solves the continuum-scale transport equations for the physiochemical processes that regulate the cell performance under various discharge conditions over a 1-D domain across the cell thickness, while calculating the rate of ion transport through spherical particles in a second radial dimension. Empirical models are employed to account for morphology effects on the material transport, and the Butler–Volmer equation is used to model the interfacial electrochemical kinetics. Although this formulation can not resolve the detailed microstructure of the electrode materials due to the homogeneity assumption, it has the advantage of being relatively computationally inexpensive, allowing a large number of simulations to populate the multidimensional design space considered in this study. Further details of the porous electrode model can be found in the original works by Doyle et al. [30, 31] and Fuller et al. [32].

2.2 Surrogate-based framework

A flow chart schematic of the surrogate modeling framework is illustrated in Fig. 1. In this study, a toolbox developed in-house for the MATLAB environment, based on the principles detailed in Refs. [33–39], is used. The following is a brief overview of the key steps to this process; further details are provided by Du et al. [29] and Queipo et al. [33].

Once the design variables, their respective ranges, and the objective functions have been defined, the next step requires constructing a design of experiments to select the set of simulations to be used for building the surrogate models.

2.2.1 *Design of experiments*

The design of experiments determines the set of design points for which the battery cell simulations are performed. The resulting data are then used to construct the surrogate models. To capture data at the extremities of the design space while also ensuring an unbiased sampling of the full range of each design variable, an approach combining face-centered composite design (FCCD) [34] and Latin hypercube sampling (LHS) [35] points is employed in this study.

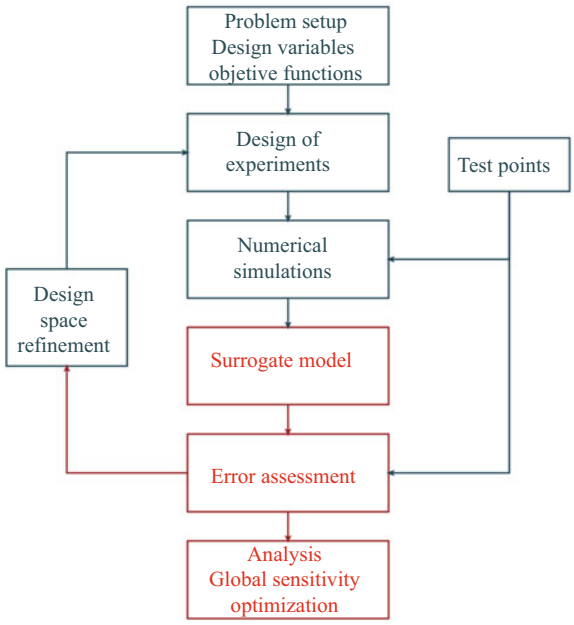

Fig. 1 Schematic of surrogate modeling framework. Processes in red are part of the MATLAB surrogates toolbox

2.2.2 *Surrogate model construction*

The data obtained from the design of experiments are used to construct surrogate models that make use of regression and interpolation techniques to approximate the objective function within the full design space. There are many types of surrogate modeling strategies available. In this study we consider polynomial response surface (PRS), kriging (KRG), and radial basis neural network (RBNN) models. The PRS models consist of a linear combination of polynomial basis functions, whose coefficients are determined using a least-squares regression approach. The KRG models consist of a combination of a low-order polynomial regression and correlation functions based on the distance from training data points in the design space [36]. The RBNN models approximate the objective function as a linear combination of Gaussian radial basis functions [37].

2.2.3 *Error assessment*

Error measures are necessary to assess the accuracy of the surrogate models. Two error assessment strategies are used in this study: prediction error sum of squares (S_{PRESS}), and independent test data. S_{PRESS} is the sum of "leave-one-out" errors, which are the errors between the true data values and those predicted from a reconstructed surrogate from all other data points from the design of experiments. Although S_{PRESS} values do not require additional data, they can be expensive to compute if the design of experiments contains a large number of data points, and may not necessarily be representative of the true error if the number of data points is small, since the surrogate model is constructed from a different design of experiments. In addition to S_{PRESS}, prediction errors at independent test points are also computed. The selection of these points requires a separate design of experiments and

simulation data. Additional validation criteria are also available for regression-based models like PRS, such as the coefficient of determination (R^2) and adjusted coefficient of determination (R^2_{adj}).

2.2.4 Further analysis

The relative magnitude of each design variable's impact on the objective function can be compared using global sensitivity analysis. An approach similar to Sobol's method [38] is implemented in this study. Global sensitivity analysis can provide insight into the design space by identifying variables of insignificant effect on the objective function. These variables can then be eliminated from consideration to reduce the problem dimensionality. Additionally, when there exist multiple competing objectives, in this case specific energy and specific power, a Pareto front can be constructed to assess the tradeoffs, e.g., how much loss in one objective must be incurred in order to improve another [39]. The Pareto front can provide important insight to the design process by identifying favorable tradeoffs between objectives under specific conditions.

2.3 Gradient-based optimization

To accurately and quickly converge to optimum design points, gradient-based optimization schemes make use of both objective function values and their derivatives. The cell optimization problem is formulated as a minimization problem, where the goal is to find the minimum of the objective function $f(x)$ subject to inequality constraints $g(x)$ and equality constraints $h(x)$

$$\begin{aligned} &\text{minimize} && f(x), && f : \mathfrak{R}^n \\ &\text{subject to} && \begin{cases} x_{\text{lower}} \leqslant x \leqslant x_{\text{upper}} & \\ g(x) \geqslant 0, & g : \mathfrak{R}^n \to \mathfrak{R}^m \\ h(x) = 0, & h : \mathfrak{R}^n \to \mathfrak{R}^k \end{cases} \end{aligned} \quad . \tag{1}$$

In this case, the objective function $f(x)$ is the gravimetric energy density obtained from the cell model. For optimization of energy density alone, there is no constraint placed on the problem. However, when two objectives are considered, such as in the case of energy and power, one of them (in this case, power) is constrained while the other is optimized.

Both the objective function and constraints specified above are nonlinear with respect to the design variables, and hence a suitable optimizer is needed. For this purpose the Sparse Nonlinear OPTimizer (SNOPT) [40], which employs a sequential quadratic programming (SQP) method to converge to the optimal solution, is selected. SQP determines its search directions for the optimal point by solving a series of quadratic programming (QP) subproblems. Each QP subproblem minimizes a quadratic approximation of the Lagrangian function subjected to linearized constraints. For the k-th QP subproblem, the quadratic function to be minimized is given by

$$\begin{aligned} &\text{minimize} && f_k + \boldsymbol{g}_k^{\mathrm{T}}(\boldsymbol{x} - \boldsymbol{x}_k) + (\boldsymbol{x} - \boldsymbol{x}_k)^{\mathrm{T}} \boldsymbol{H}_k (\boldsymbol{x} - \boldsymbol{x}_k)/2 \\ &\text{subject to} && \boldsymbol{c}_k + \boldsymbol{J}_k(\boldsymbol{x} - \boldsymbol{x}_k) = \boldsymbol{0}, \end{aligned} \tag{2}$$

where f_k is the objective function, $\boldsymbol{g}_k$ is the gradient vector, and $\boldsymbol{H}_k$ is the second-order derivative (Hessian) approximation of f_k, $\boldsymbol{c}_k$ is the vector of equality constraints, and $\boldsymbol{J}_k$ is the matrix of first-order derivatives of the constraints. Detailed explanation of the SQP method is beyond the scope of this paper; more information is provided by Gill et al. [40].

2.3.1 Computation of derivatives

One challenge to gradient-based optimization, including the SQP method used in this study, is the computation of the derivatives (gradients) of the objective function with respect to the design variables. In this study, the complex-step derivative approximation [41] is used. In spite of using complex arithmetic, this method is only applicable to real functions of real variables. To derive the complex-step derivative approximation formula, a small imaginary component is added to a real variable and a Taylor series expansion is applied

$$f(x + \mathrm{i}h) = f(x) + \mathrm{i}hf'(x) - h^2 \frac{f''(x)}{2!} + \mathrm{i}h^3 \frac{f'''(x)}{3!} + \ldots . \tag{3}$$

By taking the imaginary parts of both sides of the equation and dividing by the step size, a second order approximation of the derivative is obtained

$$f'(x) = \frac{\mathrm{Im}[f(x + \mathrm{i}h)]}{h} + O(h^2). \tag{4}$$

This concept is similar to finite-difference approximations of derivatives, but has the important advantage of being not subject to cancellation errors that limit the numerical precision in conventional finite-difference methods. In the complex-step method, derivatives can be computed to machine precision by using an arbitrarily small step size.

The second-order Hessian is not computed directly. Instead, an approximation is built using differences of the first-order derivatives. The Hessian is initialized as an identity matrix and subsequently updated using the BFGS method [42], which forces the Hessian to be symmetric and positive-definite.

2.4 Combining numerical tools

A schematic of the optimization process used in this study is illustrated in Fig. 2. Two optimization approaches can be identified: one where the gradient-based optimizer is applied to the cell model to optimize the objective function directly, and another where the surrogate framework is used to optimize the approximate surrogate function. Each of these two approaches has its own relative merits and can provide different information. When the optimizer uses output directly from the cell model instead of relying on a surrogate approximation of the objective function, the solution has one fewer source of error. Consequently, this direct approach

provides much more accurate solutions. The drawback of using the cell model directly for optimization is that the computational cost of each function evaluation is orders of magnitude greater (typically several minutes for the cell model, compared to a tenth of a second or less for the surrogate model). Preparing the optimization problem with surrogate-based analysis can significantly reduce the overall computational requirement by reducing the problem complexity via global sensitivity analysis. Additionally, in a design space with a large number of design variables each spanning a broad range of values, there are often multiple distinct physical situations of interest with unique constraints on the variables. A single surrogate model can be used for many such constrained design problems, further reducing the computational cost compared to only using the cell model for optimization. Furthermore, combining the two methods can improve the robustness by identifying discontinuities and local optima in the design space that may cause the gradient-based optimizer to converge to the incorrect solution.

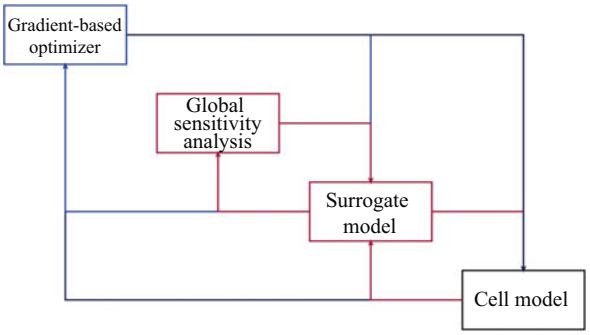

Fig. 2 Process for combining analysis and optimization tools

Given the relative advantages of these two optimization approaches, the optimization strategy adopted in this study is as follows. The surrogate models are constructed from cell model simulations. Global sensitivity analysis based on the surrogates is used to reduce the problem by modifying the bounds of certain design variables, or even eliminating them from the design space. Additional surrogate models are then constructed and refined for the reduced problem, and sample design cases are chosen for a rough optimization using the surrogate function. Finally, a few design cases of interest are selected for the final optimization using the cell model directly. When the two optimization methods are combined in this fashion, several highly accurate optimized solutions corresponding to the design scenarios of greatest interest can be obtained at a reasonable computational cost. This cannot be achieved when only one of these methods is employed independently.

3 Results and discussion

3.1 Problem setup

In the initial problem setup, the objective function of interest is the specific energy. Since it has been shown that the specific power is dominated by the effect of the cycling rate [29], power will be considered in a later section on competing objectives.

The design variables and corresponding ranges considered in this study are summarized in Table 1. Note that since the cycling rate, particle radius, and diffusion coefficient all span several orders of magnitude, they are normalized via a log-scale transformation, i.e., the value used to sample the design range and construct the surrogate models is the logarithm of the physical quantity. This allows the full range of magnitudes to be sampled and mapped. Also note that the particle radius, diffusion coefficient, electronic conductivity, and porosity apply to the cathode only; the corresponding anode properties are fixed at the values shown in Table 2. In this study, the electrodes are assumed to have a homogeneous composition, and the porosity is defined as the volume fraction of liquid in the cathode.

Table 1 Design variables and ranges

Design variable	Minimum	Maximum
Cycling rate*	C/10	10C
Particle radius*/μm	0.2	20
Diffusion coefficient*/($m^2 \cdot s^{-1}$)	1×10^{-16}	1×10^{-11}
Electronic conductivity/($S \cdot m^{-1}$)	1	10
Electrode thickness/μm	40	150
Porosity	0.2	0.4

∗ Design variables normalized via logarithmic transformation

It is important to point out the differences in problem setup between the present study and the one in Ref. [29]. As has already been mentioned, two additional variables, namely the cell porosity and cell thickness, have been included in the design of experiments. Varying these values alters the cell capacity, which was fixed in the previous study. To account for varying capacity, the anode thickness was adjusted to balance the theoretical charge capacities of the two electrodes. The reference current value used to convert between discharge current and C-rate was computed separately for each case based on the theoretical capacity of the solid electrode materials, solid volume fraction, and electrode thickness. The cells were cycled at a constant current specified by the corresponding C-rate and the simulation was terminated by reaching either a cut-off voltage of 3.0 V, or a completely discharged state in either electrode ($x = 0$ or $y = 1$). Note that this differs from the cut-off voltage of 2.0 V implemented in Ref. [29], which, in addition to being inconsistent with practical cell utilization, can be responsible for numerical instabilities in the presence of additional design variables. The specific energy was computed by integrating the voltage curve obtained from the simulation over time, and scaled by the discharge current and other appropriate constants. The specific power, although not considered in the initial design of experiments, is obtained by dividing

Table 2 Fixed parameter values for cell simulations.

Parameter	Value
Initial stoichiometric parameter for anode (x in Li_xC_6)	0.6
Initial stoichiometric parameter for cathode (y in $Li_yMn_2O_4$)	0.2
Cut-off voltage/V	3.0
Separator thickness/μm	25
Positive current collector thickness/μm	25
Negative current collector thickness/μm	25
Initial salt concentration/(mol·m^{-3})	1 000
Ambient temperature/K	298
Diffusion coefficient in anode (solid; bulk)/(m^2·s^{-1})	5.0×10^{-13}
Electronic conductivity in anode (solid; bulk)/(S·m^{-1})	100
Particle radius in anode/μm	10
Volume fraction of inert filler in cathode	0.1
Volume fraction of inert filler in anode	0.05
Anode material (solid)	MCMB 2528 graphite
Electrolyte material	$LiPF_6$ in EC:DMC
Inert filler material	PVDF

the specific energy by the total discharge time. The mass-specific values of both quantities are obtained by dividing by the cell mass, which includes the active and inactive solid, liquid, and current collectors.

3.2 Design of experiments

A design of experiments is required to systematically analyze the effects of all of the variables listed in Table 1. An initial design of experiments is performed, consisting of 77 FCCD and 600 LHS points, for a total of 677 total training data points. For error assessment, 21 test points are chosen such that the distance between test points and training data points in the design space is maximized. This is equal to 10% of the number of coefficients in a fourth-order polynomial function in six design variables. The specific energy values exhibit a wide distribution, ranging from a maximum of about 170 Wh/kg under ideal conditions (minimum cycling rate and particle size) to nearly zero for the opposite extreme (maximum cycling rate and minimum diffusivity). A total of 17 surrogate models (PRS, KRG, and RBNN) are constructed from these data. Among these, the kriging model with Gaussian correlation function is found to be the most accurate, with a normalized RMS S_{PRESS} value of 8.81% and a normalized RMS prediction error at the test points of 8.70%. Before the surrogate model is applied to perform optimization, its predictive capability can be improved by populating the design space with more data points to reduce the prediction error. In order to establish an effective strategy for refining the design of experiments, it is useful to perform global sensitivity analysis to identify design variables that can be removed, thus reducing the design space size and allowing a more efficient refinement.

3.3 Global sensitivity analysis and design space refinement

Global sensitivity indices for the aforementioned kriging model constructed from the initial design of experiments are shown in Fig. 3 and compared to results from Ref. [29], where only four design variables were considered. As reported in the previous study, a negligible contribution from the conductivity is observed. This is also confirmed by comparing the cases from the FCCD points where the conductivity was the only variable whose value is changed; in all cases varying the conductivity between the considered range causes a shift in the specific energy by less than 1%. The range of conductivity values chosen for this study reflects the conductivity of active materials already doped with carbon-additives [43], hence rendering the energy density insensitive to variations in conductivity. Figure 3 also shows that the effects of all other design variables are important. These results are again consistent with those in Ref. [29], where the thickness and porosity were not considered. In both cases the cycling rate is found to have the greatest impact on the performance of the cell, followed by the diffusivity and particle size. Note that although the main effect of porosity is also negligible, it has a non-negligible total contribution via the cross effects, and repeating the exercise by comparing FCCD points confirmed that in many cases the effect of varying the porosity over the full design range can be very significant. Based on these results, we can remove conductivity from consideration to reduce the problem dimensionality from six to five variables.

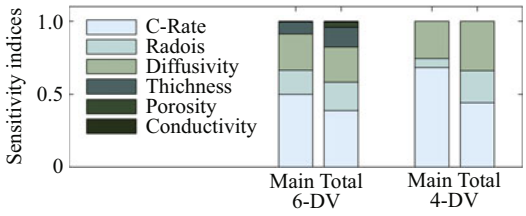

Fig. 3 Comparison of main and total sensitivity indices for designs of experiments consisting of six and four design variables

An additional 381 design points were added to the five-variable design space using an LHS filling strategy, to yield a total of 1 024 training data points. Note that some of the FCCD points are removed due to redundancy resulting from the reduction in dimensionality. Due to the higher order of polynomials that could be fit with the refined design of experiments, another 81 independent test points are also added, bringing the total to 102. This corresponds to 10% of the size of the design of experiments.

Although the design space refinement only resulted in modest improvement in the S_{PRESS} value, the prediction error at test points is substantially reduced, with the RMS value of 6.0% before the refinement reduced to 3.4% after the refinement.

3.4 Optimization of surrogate model parameters

Although the design space reduction and refinement are able to successfully improve the surrogate model's predictive capability, the errors can be reduced further by optimizing the kriging model parameters, without requiring additional training data. The Gaussian correlation function can be written as

$$R(x) = \prod_{j=1}^{n} \exp(-\theta_j d_j^2). \tag{5}$$

Typically a constant value of the correlation coefficient θ_j is used for all j

$$\theta_j = N_p^{-1/N_v}. \tag{6}$$

However, it has already been observed that the sensitivity of the objective function is quite different with respect to the various design variables, suggesting a different value of each θ_j parameter for optimal model fit. The MATLAB optimizer fmincon, an implementation of an SQP method in conjunction with the BFGS method for estimating the Hessian [42], is applied to find optimal values for the coefficients by minimizing the prediction error measure E defined as

$$E(\theta_1, \theta_2, \ldots, \theta_{N_v}) \equiv \max(\varepsilon) \sqrt{\frac{1}{N_t} \sum_{i=1}^{N_t} \varepsilon_i^2}. \tag{7}$$

Note that this measure is simply a product of the RMS and maximum prediction errors ε at the t independent test points. This measurement is selected to reduce both the RMS and maximum prediction errors, as these are the two best indicators for surrogate model accuracy. A comparison of error measures highlighting the effects of the optimization, as well as the design space reduction and refinement, is shown in Table 3.

Table 3 Comparison of error measures for kriging models from different designs of experiments

Design of experiments/Model	Initial	Reduced	Refined	Optimized
Number of design variables	6	5	5	5
Refinement level	Unrefined	Unrefined	Refined	Refined
Optimization	None	None	None	Optimized
Number of data points	677	643	1024	1024
S_{PRESS} (RMS)	0.0881	0.0655	0.0423	0.0375
RMS test prediction error	0.0870	0.0637	0.0364	0.0311
Maximum test prediction error	0.2002	0.1646	0.1057	0.0681

Table 3 shows a significant reduction in all three error measures with each iteration of the surrogate model. Although no additional points were added to the training data set from the initial design of experiments to the reduced one, decreasing the number of degrees of freedom available to the surrogate models can filter noise in the objective function.

3.5 Optimization of electrode thickness and porosity

The optimized surrogate model can be used to evaluate the effects of the design variables on the specific energy, and to identify optimal design conditions. It has been established that specific energy improves with lower cycling rate, smaller particle size, and greater diffusivity due to improved material utilization and reduced impedance. However, the effects of electrode thickness and porosity are more complicated, since they involve competing phenomena. In addition to finding the maximum value of the objective function, the surrogate model is also used to explore the dependence of optimal values of certain design variables with respect to other variables. For instance, we are interested in not only

the optimal electrode thickness and porosity under a specific given scenario, but also the dependence of this optimum on the other design variables.

Examples of the objective function plotted over 1-D sweeps of the design space are shown in Fig. 4. The specific energy predicted by the surrogate model over the range of electrode thicknesses is plotted for different discrete values of each design variable. The plots in Fig. 4 show that not only does the functional dependence of the specific energy on electrode thickness vary with the values of the other variables, but the optimal thickness varies as well. Note that the plots shown in Fig. 4 are only a few examples plotted over selected sweeps of the design space and are not representative of the overall multidimensional space. This illustrates the difficulty of optimizing an electrode's thickness, since the operating conditions (e.g., discharge rate) vary during the cell's life and the material properties (e.g., particle size and diffusivity) are non-homogeneous and vary within the electrode.

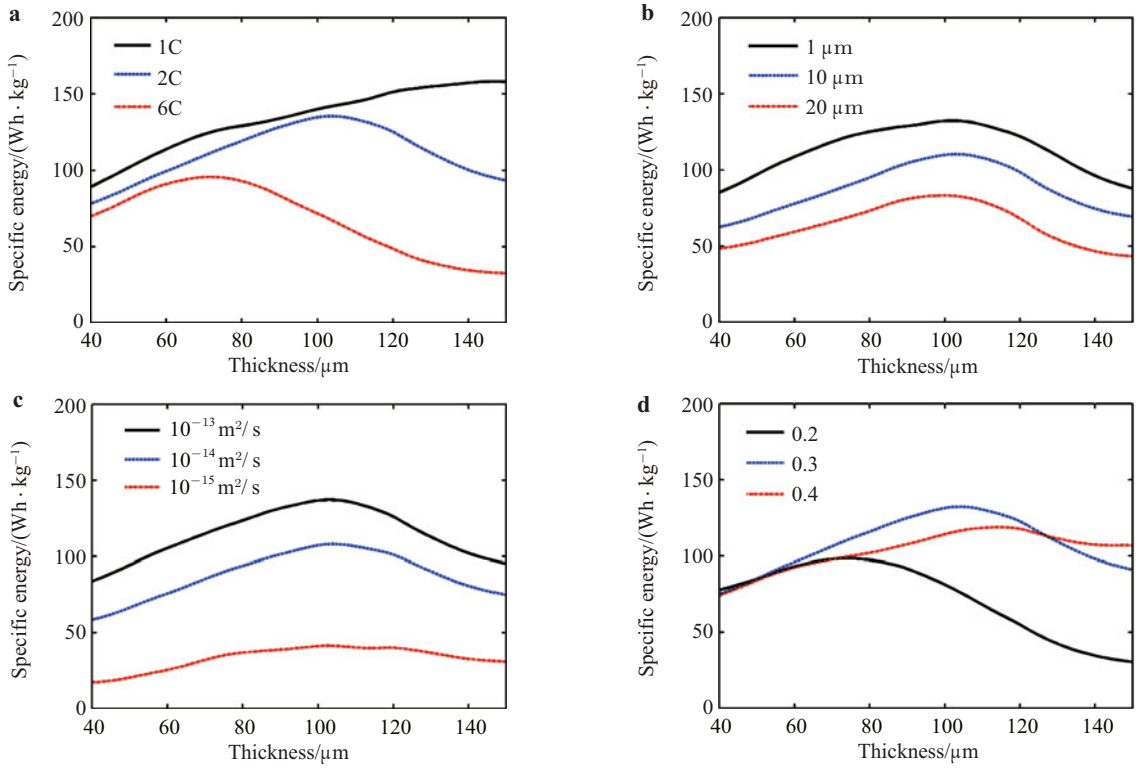

Fig. 4 Dependence of optimal thickness on **a** cycling rate; **b** particle radius; **c** diffusion coefficient; **d** porosity

Table 4 Fixed design conditions for optimization cases

Case number	C-rate	Particle radius/μm	Diffusion coefficient/($m^2 \cdot s^{-1}$)
1	C/10	0.2	1×10^{-12}
2	2C	2	1×10^{-14}
3	10C	2	1×10^{-14}

To examine the effect of cycling rate, particle size, and diffusivity on the optimal thickness and porosity of the electrode in greater detail, we consider three cases summarized in Table 4. Since bounds on the design variables have been specified, the optimization is conducted with both gradient-based (using direct data from the cell model) and surrogate-based methods. For the surrogate model, the optimum is again found using fmincon. This is a similar approach to the method used by the gradient-based optimizer, applied to the surrogate model instead of the cell data. These three cases correspond to significantly different design scenarios, and are selected to demonstrate the capabilities of the optimization methods and to compare their performance.

Case 1 is a situation in which the characteristic diffusion time, as defined in Ref. [29], is much smaller than the discharge time due to the small particle size and high diffusion coefficient, so the cell is not limited by the diffusion rate. In Cases 2 and 3, the diffusion coefficient is much smaller and the particle size is much larger, so diffusion becomes a limiting factor in the cell performance. Case 2 models a high cycling rate corresponding to a high performance situation for a vehicle. Case 3 models the maximum discharge rate scenario.

Contour plots of the objective function over the full electrode thickness and porosity ranges for Cases 1–3 are shown in Figs. 5–7, along with the location of the optimum de-

sign for maximizing the specific energy. To assess the accuracy of the surrogate model and compare the accuracy of the two methods, contour plots of the relative difference between the actual cell data and predicted output from the surrogate model are also shown. In Case 1, both optimization methods found the optimum at the lower right corner, i.e., at the upper bound of the thickness and lower bound of the porosity. This indicates that the thickest electrode with minimum porosity (and thus maximum solid volume fraction) is preferred. Since the diffusion rate is not a limiting factor in this case, greater energy can be extracted by increasing the amount of active solid material in the electrode. Although the two methods converge to the same solution in the design space, they yield different objective function values. Since the gradient-based method uses data directly from the cell model, its final solution is also the true optimum. In this case, the surrogate model overestimates the specific energy by 6.4%. Case 1 demonstrates that even when the surrogate model can be used to predict the correct optimum, the function value still contains uncertainty due to prediction error in the surrogate model.

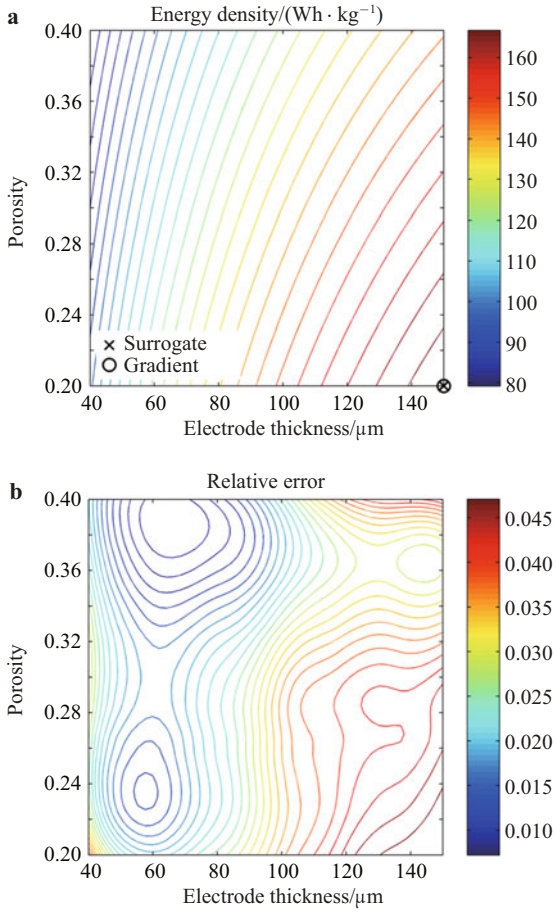

Fig. 5 Contour plot of specific energy (Wh/kg) against electrode thickness and porosity for Case 1 (high diffusion, low C-rate). Normalized difference between surrogate-based (δ = 150.0 μm, ε = 0.200, E = 181.4 Wh/kg) and gradient-based optimum (δ = 150.0 μm, ε = 0.200, E = 170.4 Wh/kg) is 6.4%

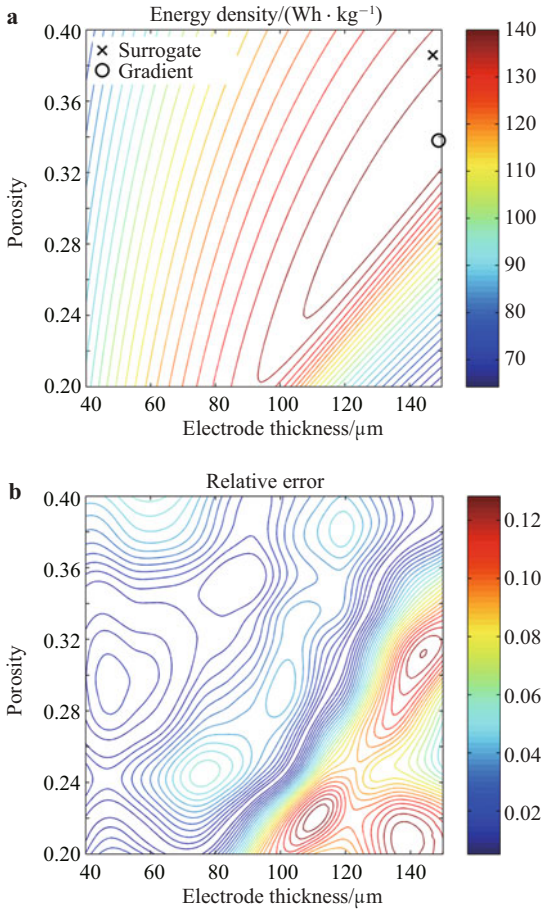

Fig. 6 Contour plot of specific energy (Wh/kg) against electrode thickness and porosity for Case 2 (low diffusion, high C-rate). Normalized difference between surrogate-based (δ = 147.3 μm, ε = 0.386, E = 138.9 Wh/kg) and gradient-based optimum (δ = 149.0 μm, ε = 0.338, E = 143.2 Wh/kg) is 2.5%

In contrast to Case 1, the diffusion rate is a limiting factor in Case 2, and the optimal design region from Case 1 shows poor performance in Case 2. In this scenario, the characteristic diffusion time is not significantly shorter than the discharge time, and much of the active material of a thick, dense electrode cannot be utilized. Instead, the optimum is located near the top right corner, indicating that a thick electrode is still favored, but a much higher porosity is needed to ensure proper utilization of the thick electrode under these conditions. Unlike in the previous case, the two methods converge to different solutions in the design space. However, despite this difference, the final energy density values differ by only 2.5%, suggesting that the optimum lies in a flat region of the design space where the objective function is not sensitive to the design variables. This is supported by the contour plot in Fig. 6, which shows a large region where over 90% of the maximum energy density can be achieved. The shape of contours in Fig. 6 also show that to achieve good performance, some the electrode must be made either thinner or more porous, suggesting that the diffusion rate is a performance limitation in this case. We also note that the

energy density values are much lower than in Case 1, which is consistent with results in Ref. [29].

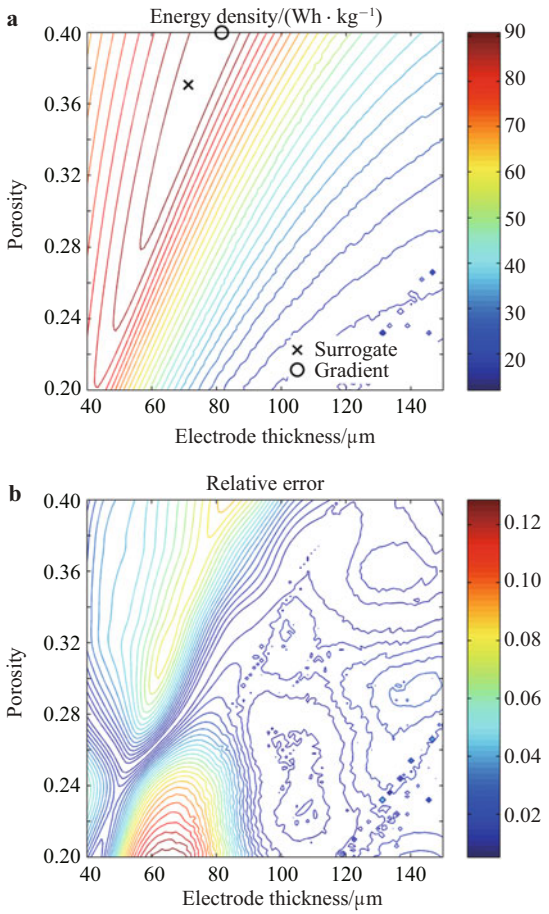

Fig. 7 Contour plot of specific energy (Wh/kg) against electrode thickness and porosity for Case 3 (low diffusion, maximum C-rate). Difference between surrogate-based (δ = 71.2 μm, ε = 0.371, E = 80.6 Wh/kg) and gradient-based optimum (δ = 81.5 μm, ε = 0.400, E = 94.1 Wh/kg) is 7.9%

Case 3 shows that for very high cycling rates, a much thinner electrode is required, and porosity is the limiting factor. The specific energy values are also significantly lower than those in Case 2, indicating a further loss of capacity utilization as the cycling rate is increased. The locations of the optima found by the two methods agree well with each other, with a difference of 7.9% in the solutions. The shape of the contour lines suggests that the region near the solution is more sensitive to the design variables in this case, and thus a great penalty is incurred for sub-optimal design. We also note that Figs. 5–7 show that in all three cases, the specific energy appears to vary much more with changes in the electrode thickness than with changes in the porosity. This is an indication of greater sensitivity to the thickness, and is consistent with the results shown in Fig. 3.

These results are consistent with the established practice of using thick electrodes in high energy applications and thin electrodes in high power applications. However, although only three cases are shown here, the surrogate model maps the entire design space and is therefore able to optimize the design variables under consideration for any combination of other inputs (i.e. for any number of "intermediate" situations). The relative error contours in Figs. 5–7 show that the prediction error of the surrogate model is less than 5% in the majority of the design space, but can be 10% or greater in a few isolated pockets. This demonstrates that the two methods each have their own advantages, and are ultimately complementary: the surrogate model provides computationally cheap approximations of the objective function, allowing for an efficient analysis of the full design space and a rough optimization. However, the gradient-based optimizer is required to refine the optimization solution to machine precision. In turn, a global mapping of the design space provided by the surrogate model complements the accuracy of the gradient-based optimizer to provide better insight into the physical phenomena being modeled.

3.6 Power-energy tradeoff

The analysis presented so far has focused on the specific energy. However, in real applications, a cell must be designed to provide not only adequate energy, but also adequate power. To provide a proper context for our results concerning specific energy, we consider the tradeoff between specific energy and specific power. Rather than considering a sequence of individual optimization problems with varying power constraints, the entire spectrum of power and energy ranges can be modeled at once by constructing separate surrogate models for the specific power.

Previous work [29] studying the power-energy trade within a surrogate modeling framework considered four design variables corresponding to the cathode. It was found that the Pareto front quantifying the tradeoff between maximum achievable specific power and energy allowed large gains in power for small sacrifices in energy. However, the maximum C-rate considered was 4, thus limiting the maximum power level. A comparison of the Pareto fronts for the data from the current study with those from Ref. [29] is shown in Fig. 8.

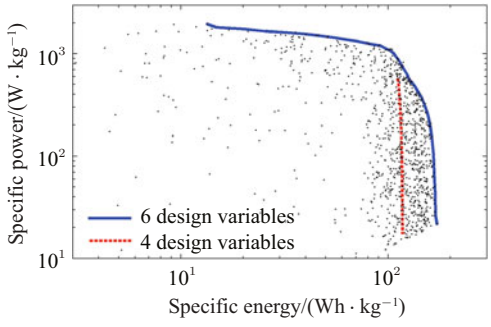

Fig. 8 Comparison of Pareto fronts for specific power vs. specific energy for current study (6 design variables, Max C-rate is 10), and Ref. [29] (4 design variables, Max C-rate is 4)

The specific energy values shown for the 4-variable case in Fig. 8 are adjusted to account for the different state-of-charge (SOC) windows modeled in the two sets of simulations. The inclusion of two additional design variables allowed significant gains (up to 40% in low-power regions) in energy. This is consistent with the results in Figs. 5–7 highlighting the importance of matching the electrode thickness to the physical situation being modeled.

Naturally, increasing the maximum cycling rate also allows much higher power levels to be realized, although at a heavy penalty in specific energy due to poor utilization. In fact, the results at high power levels are in direct contrast to those from Ref. [29], which found a steep Pareto front that shows high achievable power with minimal loss in energy. The new results with 6 design variables suggest a critical point corresponding to power and energy levels of approximately 1000 W/kg and 100 Wh/kg, respectively, above which additional gains in power are accompanied by an unavoidable losses in energy. The C-rate corresponding to this critical power level depends on the values of the electrode thickness and porosity, but is typically between 6C and 8C. The quantification of the relationship between achievable power and energy is necessary for scaling the cell optimization to a pack-level optimization, as it provides guidelines for distributing the required current load among multiple cells.

4 Conclusions

In this study, we have successfully developed a gradient- and surrogate-based framework to analyze and optimize battery cells using a cell-level model. In this framework, surrogate models capable of predicting the specific energy provided by a cell during discharge for given operational, morphological, and material-dependent parameters have been constructed and utilized to observe the competing effects of different design variables. Based on the global perspective provided by the surrogate model, key operating scenarios were identified, and optimal designs were identified under these operating conditions using multiple optimization techniques. The relative impact of the design variables has also been established, and comparing the competing objectives of specific energy and specific power has identified distinct regions of the design space where different objectives are favored.

Generally, the specific energy was found to decrease for higher cycling rates, larger particle size, and lower diffusivity as expected. The effect of electrode thickness is much more complicated, with an optimal thickness that varies greatly depending on the values of the other design variables. The porosity was found to have a lesser but non-negligible influence on the specific energy, and its optimal value also strongly depends on the values of the other parameters. These complicated interactions between design variables illustrate the difficulty of cell optimization, and can help explain why even optimized cells may perform poorly under different operating conditions. The electrode thickness and porosity were optimized simultaneously using a gradient-based optimization method for three distinct physical situations, and it was found that the optimal thickness decreases substantially as the characteristic diffusion time (defined in Ref. [29]) and the cycling rate are increased.

A comparison between the optimization results obtained using surrogate-based and gradient-based methods shows that optimizing a surrogate function in lieu of the true objective function yields optimization solutions to within a 5% error margin. Although this is insufficient for many design problems, the ability to perform approximate optimization for a large number of design cases and multiple objectives, as well as constrain the design space via global sensitivity analysis, makes the surrogate method a valuable intermediate step between problem formulation and the final design optimization. Once the most important design cases have been identified, the gradient-based optimizer can be applied directly to the physical model to obtain a much more accurate solution by using exact function and gradient information at each iteration, bypassing surrogate model prediction errors. Within the current modeling framework, the two optimization methods are complementary and can provide accurate optimized solutions for multiple distinct physical scenarios for a reasonable computational cost.

One simplification in this work is the inclusion of only the cell components in calculating the battery mass used to normalize the total energy and power output. An actual battery system will require packaging and other components which may contribute significantly to the total mass of the system. Another limitation to the current methodology is the assumption of homogeneous electrode composition in the porous electrode model, which prevents us from incorporating the effects of a detailed microstructure. The analysis is also limited to uniformly sized, spherical particles, and although Zhang et al. [13] have shown that particle shape has an insignificant effect on stress for the range of materials considered, the present model does not capture the effects of polydisperse particle size distributions. However, the surrogate modeling framework is more general and can be applied to any physical model. Efforts are currently underway to improve the existing cell model by incorporating physics-based models for the effective material properties based on non-homogeneous microstructures [15].

Acknowledgement The present efforts were supported by the General Motors and University of Michigan Advanced Battery Coalition for Drivetrains (ABCD).

References

1 Grasmeyer, J. M., Keennon, M. T.: Development of the black widow micro air vehicle. In: Mueller TJ (ed) Fixed and flapping wing aerodynamics for micro air vehicle applications. (Progress in astronautics and aeronautics) AIAA Reston Vol. 195, VA (2001)

2 Lu, C. H., Lin, S. W.: Influence of the particle size on the electrochemical properties of lithium manganese oxide. J. Power Sources **97**, 458–460 (2001)

3 Drezen, T., Kwon, N. H., Bowen, P., et al.: Effect of particle size on $LiMnPO_4$ cathodes. J. Power Sources **174**, 949–953 (2007)

4 Tran, T. D., Feikert, J. H., Pekala, R.W., et al.: Rate effect on lithium-ion graphite electrode performance. J. Applied Electrochem. **26**, 1161–1167 (1996)

5 Garcia, R. E., Chiang, Y. M., Carter, W. C., et al.: Microstructural modeling and design of rechargeable lithium-ion batteries. J. Electrochem. Soc. **152**, A255–A263 (2004)

6 Darling, R., Newman, J.: Modeling a porous intercalation electrode with two characteristic particle sizes. J. Electrochem. Soc. **144**, 4201–4208 (1997)

7 Ahn, S., Kim, Y., Kim, K. J., et al.: Development of high capacity, high rate lithium ion batteries utilizing metal fiber conductive additives. J. Power Sources **81**, 896–901 (1999)

8 Haran, B., Popov, B. N., White, R. E.: Determination of the hydrogen diffusion coefficient in metal hydrides by impedance spectroscopy. J. Power Sources **75**, 56–63 (1998)

9 Santhanagopalan, S., Guo, Q., White, R. E.: Parameter estimation and model discrimination for a lithium-ion cell. J. Electrochem. Soc. **154**, A198–A206 (2007)

10 Verbrugge, M. W., Conell R. S.: Electrochemical and thermal characterization of battery modules commensurate with electric vehicle integration. J. Electrochem. Soc. **149**, A45–A53 (2002)

11 Liaw, B. Y., Nagasubramanian, G., Jungst, R. G., et al.: Modeling of lithium ion cells—a simple equivalent-circuit model approach. Solid State Ionics **175**, 835–839 (2004)

12 Ramadass, P., Haran, B., White, R. E., et al.: Mathematical modeling of the capacity fade of Li-ion cells. J. Power Sources **123**, 230–240 (2003)

13 Zhang, X., Shyy, W., Sastry, A. M.: Numerical simulation of intercalation-induced stress in Li-ion battery electrode particles. J. Electrochem. Soc. **154**, A910–A916 (2007)

14 Zhang, X., Sastry, A. M., Shyy, W.: Intercalation-induced stress and heat generation within single lithium-ion battery electrode particles. J. Electrochem. Soc. **155**, A542–A552 (2008)

15 Gupta, A., Seo, J. H., Zhang, X., et al.: Effective transport properties of LiMn2O4 electrode via particle-scale modeling. J. Electrochem. Soc. **158**, A487–A497 (2011)

16 Wang, C. W., Sastry, A. M.: Mesoscale modeling of a Li-ion polymer cell. J. Electrochem. Soc. **154**, A1035–A1047 (2007)

17 Ramadesigan, V., Boovaragavan, V., Pirkle, J. C., et al.: Efficient reformulation of solid-phase diffusion in physics-based lithium-ion battery models. J. Electrochem. Soc. **157**, A854–A860 (2010)

18 Northrop, P. W. C., Ramadesigan, V., De, S., et al.: Coordinate transformation, orthogonal collocation, model reformulation and simulation of electrochemical-thermal behavior of lithium-ion battery stacks. J. Electrochem. Soc. **158**, A1461–A1477 (2011)

19 De, S., Northrop, P. W. C., Ramadesigan, V., et al.: Model-based simultaneous optimization of multiple design parameters for lithium-ion batteries for maximization of energy density. J. Power Sources **227**, 161–170 (2013)

20 Ramadesigan, V., Northrop, P. W. C., De, S., et al.: Modeling and simulation of lithium-ion batteries from a systems engineering perspective. J. Electrochem. Soc. **159**, R31–R45 (2012)

21 Srinivasan, V., Newman, J.: Design and optimization of a natural graphite/iron phosphate lithium-ion cell. J. Electrochem. Soc. **151**, A1530–A1538 (2004)

22 Stephenson, D. E., Hartman, E. M., Harb, J. H., et al.: Modeling of particle-particle interactions in porous cathodes for lithium-ion batteries. J. Electrochem. Soc. **154**, A1146–A1155 (2007)

23 Fletcher, R., Powell, M. J. D.: A rapidly convergent descent method for minimization. The Computer Journal **6**, 163–168 (1963)

24 Nelder, J. A., Mead. R.: A simplex method for function minimization. The Computer Journal **7**, 308–313 (1965)

25 Kennedy, J., Eberhart, R.C.: Particle swarm optimization. Proceedings of IEEE international conference on neural networks **4**, 1942–1948 (1995)

26 Zingg, D. W., Nemec, M., Pulliam, T. H.: A comparative evaluation of genetic and gradient-based algorithms applied to aerodynamic optimization. REMN **17**, 103–126 (2008)

27 Shyy, W., Cho, Y. C., Du, W., et al.: Surrogate-based modeling and dimension reduction techniques for multi-scale mechanics problems. Acta Mechanica Sinica **27**, 845–865 (2011)

28 Tseng, C., Shyy, W.: Modeling for isothermal and cryogenic cavitation. Int. J. Heat and Mass Transfer **53**, 513–525 (2010)

29 Du, W., Gupta, A., Zhang, X., et al.: Effect of cycling rate, particle size and transport properties on lithium-ion cathode performance. Int. J. Heat and Mass Transfer **53**, 3552–3561 (2010)

30 Doyle, M., Fuller, T. F., Newman, J.: Modeling of galvanostatic charge and discharge of the lithium/polymer/insertion cell. J. Electrochem. Soc. **140**, 1526–1533 (1993)

31 Doyle, M., Newman, J., Gozdz, A.S., et al.: Comparison of modeling predictions with experimental data from plastic lithium ion cells. J. Electrochem. Soc. **143**, 1890–1903 (1996)

32 Fuller, T. F., Doyle, M., Newman, J.: Simulation and optimization of the dual lithium ion insertion cell. J. Electrochem. Soc. **141**, 1–10 (1994)

33 Queipo, N. V., Haftka, R. T., Shyy, W., et al.: Surrogate-based analysis and optimization. Prog. Aero. Sci. **41**, 1–28 (2005)

34 McKay, M. D., Beckman, R. J., Conover, W. J.: Comparison of three methods for selecting values of input variables in the analysis of output from a computer code. Technometrics **21**, 239–245 (1979)

35 Myers, R. H., Montgomery, D. C.: Response Surface Methodology: Process and Product in Optimization Using Designed Experiments. Wiley and Sons Inc., New York, New York (1995)

36 Lophaven, S. N., Nielsen, H. B., Sondergaard, J.: DACE—A Matlab kriging toolbox. Version 2.0, Technical Report, IMM-TR-2002-12, Technical University of Denmark, Denmark (2002)

37 Goel, T., Dorney, D. J., Haftka, R. T., et al.: Improving the hydrodynamic performance of diffuser vanes via shape optimization. Computers & Fluids **37**, 705–723 (2008)

38 Sobol, I.: Global sensitivity indices for nonlinear mathematical models and their Monte Carlo estimates. Mathematics and Computers in simulation 55, 271–280 (2001)

39 Mack, Y., Goel, T., Shyy, W., et al.: Surrogate Model-based Optimization Framework: A Case Study in Aerospace Design. In: Yang S, Ong YS, Jin Y (eds) Evolutionary computation in dynamic and uncertain environments. (Studies in computational intelligence) Springer, Berlin Heidelberg New York, 323–342 (2007)
40 Gill P. E., Murray, W., Saunders, M.A.: SNOPT: an SQP algorithm for large-scale constrained optimization. SIAM Journal on optimization **12**, 979–1006 (2002)
41 Martins, J. R. R. A., Sturdza, P., Alonso, J.J.: The complex-step derivative approximation. ACM Transactions on Mathematical Software **29**, 245–262 (2003)
42 Powell, M. J. D.: A fast algorithm for nonlinearly constrained optimization calculations. In: Watson GA (ed) Lecture notes in mathematics. (Numerical analysis) Springer, Berlin Heidelberg New York, 144–157 (1978)
43 Chen, Y. H., Wang, C. W., Zhang, X., et al.: Porous cathode optimization for lithium cells: Ionic and electronic conductivity, capacity, and selection of materials. J. Power Sources, **195**, 2851–2862 (2010)